Journal of Inorganic Biochemistry 230 (2022) 111764

Contents lists available at ScienceDirect

Journal of Inorganic Biochemistry

journal homepage: www.elsevier.com/locate/jinorgbio

Aptamer versus antibody as probes for the impedimetric biosensor for human epidermal growth factor receptor

Sixolile Centane, Tebello Nyokong *

Institute for Nanotechnology Innovation, Rhodes University, Chemistry Department, PO Box 94, Makhanda 6140, South Africa

ARTICLE INFO

Keywords:
Aptasensors
Immunosensors
Human epidermal growth factor receptor
HB5 aptamer
Trasmatuzab

ABSTRACT

In the present work, the performance of aptamer and antibody bioreceptors for the detection of the human epidermal growth factor receptor (HER2) cancer biomarker on a glassy carbon electrode is reported. The carboxylic acid group rich graphene quantum dots (GQDs) modified with gold nanoparticles and a porphyrin binuclear framework (CoP-BNF) were used to modify the glassy carbon electrode. The aptamer and antibody were both amine functionalized and attached to GQDs and CoP-BNF through an amide bond. The designed immunosensors and aptasensors in this work were characterized using electrochemical impedance spectroscopy. The aptasensors, compared to the immunosensors gave better limit of detection values. The aptasensor outperforms the immunosensor in terms of its reusability and storability, while the immunosensor could not be regenerated for subsequent experiments. The potential applicability of all sensors in this work was also investigated, by detection of HER2 in spiked human serum with acceptable results.

1. Introduction

The distinguishing factor of biosensors compared to any other sensor, is molecular recognition. Antigen–receptor interaction, is a fundamental step and component in various biological systems, molecular therapy, clinical diagnosis, biosensors and biotechnologies [1,2]. A molecular recognition element takes part in the recognition process, and provides a receptor site for the attachment of an antigenic molecule [3]. Aptamer and antibodies are part of these recognition elements. Antibodies are a blood protein produced by the immune system in response to and counteracting a specific antigen [4,5]. Antibodies combine chemically with substances which the body recognizes as alien, such as bacteria, viruses, and foreign substances in the blood. Since their first discovery, there has been exhaustive research on antibodies as recognition elements in biosensor design, with favourable limit of detection values and sensitivity [5,6]. Even so, antibodies have shown some limitations in biosensor design such as, poor specificity for small targets, failure to recognize targets under non-physiological conditions, lack of quality, stability and reproducibility [7,8]. Aptamers are short, single-stranded deoxyribonucleic acid (ssDNA) or ribonucleic acid (ssRNA) molecules that can selectively bind to a specific target, including proteins, peptides, carbohydrates, small molecules, toxins, and even live cells [9,10]. Similar to the antibody-antigen interaction, the recognition between aptamers and their target is very specific. The selectivity of the aptamer is due to its three dimensional structure, which allows it to specifically bind the target via non-covalent interaction [10]. Owing to these properties aptamers have been widely investigated as an alternative to antibodies in therapeutics and diagnostics. Aptamers are seen as potential replacements for these antibodies. Compared to antibodies, aptamers are stable even in non-physiological pH conditions, and are generated in less expensive and less invasive conditions. In addition, aptamers are smaller in size, have a much more flexible nature, and have better conductivity than antibodies [11–14]. Various reports are available on bioassays using either antibodies or aptamers as recognition elements towards a specific antigen. A few reports exist on the comparative study on aptasensors and immunosensors under equivalent conditions. The performance of an aptamer and monoclonal antibody was directly compared for the detection of a prostate specific antigen on screen printed carbon electrodes [15]. Another study comparing the performance of aptamers and an antibody is reported by Yao et al., where an antibody and aptamer specific for immunoglobulin E were immobilized on a gold surface of quartz crystal microbalance [16]. On the other hand, Schlecht et al. also showed a comparison of antibody and aptamer receptors for the specific detection of thrombin with a nanometer gap-sized impedance biosensor made on gold electrodes [17]. An enzyme linked immunosorbent assay-based format was used to directly

* Corresponding author.
E-mail address: t.nyokong@ru.ac.za (T. Nyokong).

https://doi.org/10.1016/j.jinorgbio.2022.111764
Received 8 October 2021; Received in revised form 8 February 2022; Accepted 9 February 2022
Available online 14 February 2022

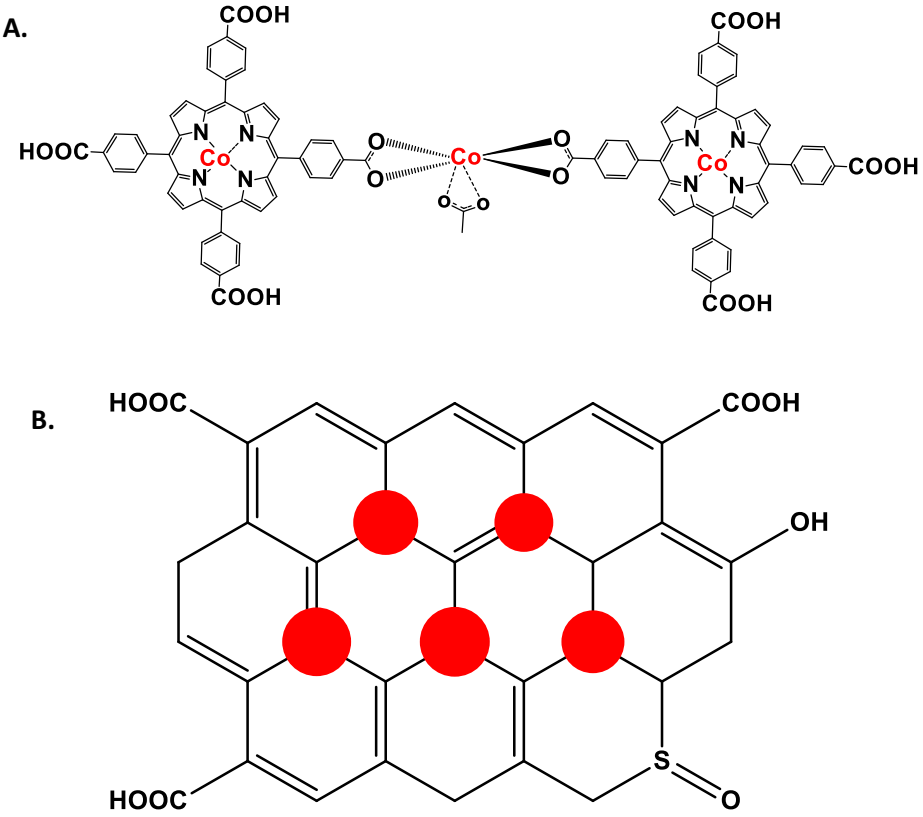

Fig. 1. The structure of the nanomaterials used in this work. The cobalt porphyrin binuclear framework (A) and the sulfur and nitrogen doped graphene quantum dots (SNGQDs@AuNPs) (B).

compare the performance of a newly selected aptamer for human noroviruses and a commercially available antibody [18]. In all four comparative studies, the aptasensors showed superiority in terms of better stability, simplicity, regeneration and cost effectiveness. Co porphyrin binuclear framework (CoP-BNF) modified (represented as CoP-BNF/SNGQDs@AuNPs) modified glassy carbon electrode is employed in this work for the detection of the human epidermal growth factor receptor (HER2). In our previous work [19] we have shown the performance of the Trastuzumab (anti-HER2 antibody), towards the electrochemical detection of HER2. In the present work, for the first time we focus on the performance of the aptasensor, using an HER2 specific aptamer (HB5) instead of an antibody. To the best of our knowledge, this is first comparative study of aptasensor and immunosensor towards the detection of HER2. The roles of each of the components of the employed platform (CoP-BNF/SNGQDs@AuNPs) are as follows: The immobilization of Au nanoparticles (AuNPs) onto GQDs has been reported to prevent the aggregation of the latter [20]. Sulfur/nitrogen doped GQDs (SNGQDs) are employed since the introduction of S and N into GQDs causes the synergistic effect of N and S, which facilitates the electron transfer, hence improving electrocatalysis [21]. Porphyrins are aromatic compounds which are electroactive [22], and have good structural flexibility. Their properties can be fine-tuned to suit the desired application [23]. Polymeric porphyrins are known for improved electrocatalytic activity [24], hence CoP-BNF is employed. In addition, a porphyrin-based covalent organic framework has been used to immobilize aptamer strands for the detection of epidermal growth factor receptor [25]. The cobalt based binuclear framework, compared to any other porphyrin related structures has two cobalt metal centers, which results in enhanced redox activity and electron transfer. Furthermore, because of the binuclear structure more carboxylic groups are present to provide more sites for the immobilization of the HB5 and Trasmatuzab biorecognition elements for improved sensitivity of the sensors designed. Even though porphyrin organic frameworks have been employed for HER2 detection [25], in this work we employ a simpler binuclear porphyrin, which has been reported to preserve the networking [26].

2. Materials and methods

2.1. Materials

The following materials were purchased Sigma Aldrich: human serum, bovine serum albumin (BSA), N-hydroxy succinimide (NHS), 1-ethyl-3-(3-dimethylaminopropyl) carbodiimide (EDC), Na_2HPO_4, KH_2PO_4, NaCl, KCl, $K_4[Fe(CN)_6]$, $K_3[Fe(CN)_6]$, the protein (human epidermal growth factor receptor 2, HER2) and the monoclonal antibody, Trastuzumab. The HB5 DNA aptamer (5′−/5 AmMC6/AAC CGC CCA AAT CCC TAA GAG TCT GCA CTT GTC ATT TTG TAT ATG TAT TTG GTT TTT GGC TCT CAC AGA CAC ACT ACA CAC GCA CA-3′) was purchased from Integrated DNA Technologies, South Africa. Phosphate buffer saline (PBS, pH 7.4) was prepared using weighed amounts of Na_2HPO_4, KH_2PO_4, KCl and NaCl. Millipore water was obtained from an Elga PURELAB Chorus 2 system. SNGQDs@AuNPs, CoP-BNF and glassy carbon electrode (GCE) modification with both (GCE/CoP-BNF/SNGQDs@AuNPs) were as outlined in our previous work with no modification [19].

2.2. Equipment

Electrochemical impedance spectroscopy (EIS) and cyclic voltammetry (CV) studies were performed using an Autolab Potentiostat PGSTAT30 equipped with Nova software version 2.1. The EIS experiments were performed between 0.1 and 10 kHz, using a 5 mV/rms sinusoidal modulation and alternating current potential of 0.24 V. A non-

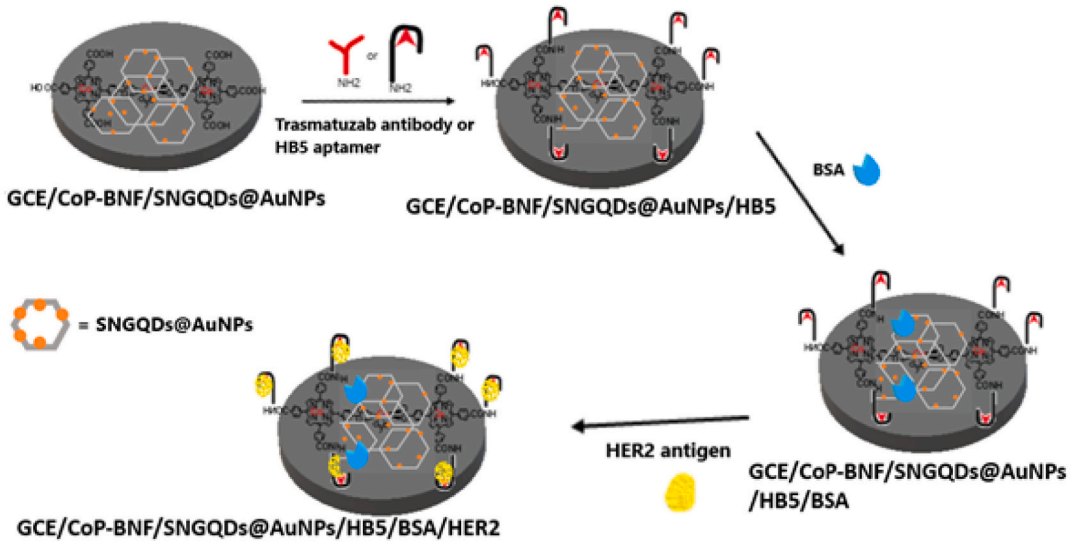

Scheme 1. Steps towards the fabrication of the sensors in this work. The figure shows the probe GCE/CoP-BNF/SNGQDs@AuNPs as an example.

linear least squares method based on the EQUIVCRT programme was used for automatic fitting of the obtained EIS data. X-ray photoelectron spectroscopy (XPS) spectra were collected using a Kratos Axis Ultra delay-line detector, using an Al (monochromatic) anode, equipped with charge neutralizer and the operating pressure kept below 5.0×10^{-9} Torr. For wide/survey XPS scans, the following parameters were used: emission current was kept at 5 mA and the anode voltage at 15 kV. The resolution used to acquire wide/survey scans was at 160 eV pass energy using a hybrid lens in the slot mode. For high resolution scans, the resolution was changed to 40 eV pass energy in the slot mode. Curve fitting was performed using Gaussian-Lorentzian peak shape after performing a linear background correction. Glassy carbon plates (GCP, Goodfellow, UK, 1 × 1 cm and 2 mm thick) were used for XPS.

2.3. Electrode modification

All the solutions were freshly prepared in Milli-Q water and stored at the temperature of 4 °C until use. The structure of both the SNGQDs@AuNPs and CoP-BNF nanomaterials are shown in Fig. 1. (See Scheme 1.)

Solutions were deaerated by bubbling argon gas prior to the electrochemistry experiments and the electrochemical cell was kept under argon atmosphere throughout the experiments. A glassy carbon electrode was first polished with Al_2O_3 powder (Aldrich, 0.1, 0.05 mm) using Metrohm polishing kit, and rinsed with deionized water, followed by sonication in ethanol and deionized water. Finally, the electrode was allowed to dry at room temperature. All the GCEs were modified by the drop dry methods where the modifier was dropped on the electrode followed by drying. The first GCE was modified with CoP-BNF (10 µL, 2 mg, 0.00175 mmol in aqueous solution), and left to dry in the oven, represented as GCE/CoP-BNF. The second electrode was modified with the SNGQDs@AuNPs (10 µL, 2 mg/mL in aqueous solution), left to dry in the oven and is represented as GCE/SNGQDs@AuNPs. The third electrode was modified with both CoP-BNF and SNGQDs@AuNPs sequentially (using the same amounts as above and is represented as GCE/CoP-BNF/SNGQDs@AuNPs, where the CoP-BNF was placed first on the GCE followed by SNGQDs@AuNPs. There were six modified electrodes: three contained the HB5 aptamer, the other three contained the Trasmatuzab antibody. The electrodes were modified with Trasmatuzab or HB5 through formation of an amide bond following activation

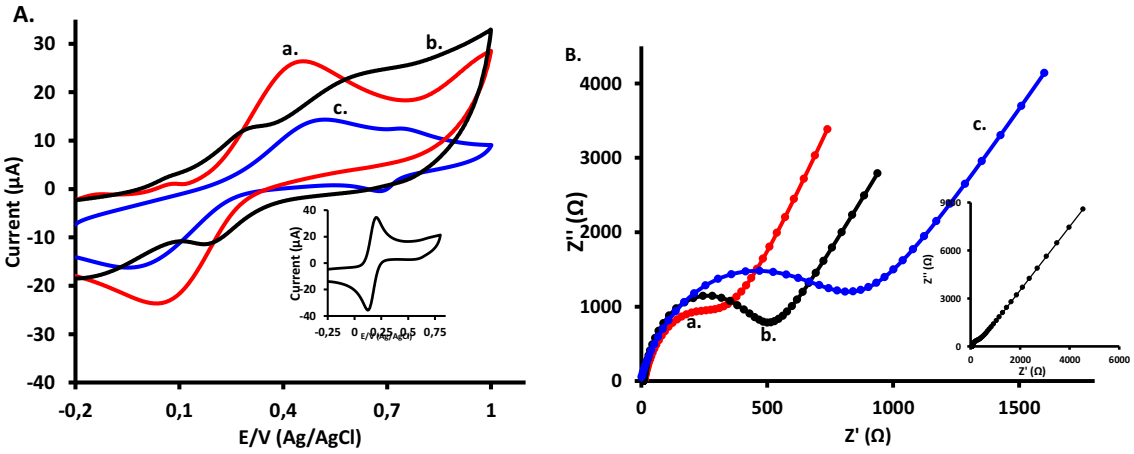

Fig. 2. Cyclic voltammogram (A) and Nyquist plots (B) for the modified electrodes. (a) GCE/SNGQDs@AuNPs, (b) GCE/CoP-BNF/ SNGQDs@AuNPs and (c) GCE/CoP-BNF. All in 1 mM $Fe(CN)_6]^{3-/4-}$ in 0.1 mol·L^{-1} KCl. Inserts = bare GCE.

Table 1
Data obtained for the probes in 1 mM $Fe(CN)_6]^{3-/4-}$ in 0.1 mol·L^{-1} KCl in 10 mM PBS (pH 7.4). Values in brackets are the detection of HER2 at 6 ng/mL.

Probes	ΔEp (mV)	R_{ct} (Ω)
GCE	68	185
GCE/SNGQDs@AuNPs	386	381
GCE/SNGQDs@AuNPs/HB5	–	2170 (7267)
GCE/SNGQDs@AuNPs/Trasmatuzab	–	1923 (5620)
GCE/CoP-BNF	555	838
GCE/CoP-BNF/HB5	–	943 (1757)
GCE/CoP-BNF/Trasmatuzab	–	1770 (3503)
GCE/CoP-BNF/SNGQDs@AuNPs	437	808
GCE/CoP-BNF/SNGQDs@AuNPs/HB5	–	1230 (8972)
GCE/CoP-BNF/SNGQDs@AuNPs/Trasmatuzab	–	3080 (13666)

via EDC/NHS coupling as follows: Each electrode (GCE/CoP-BNF, GCE/SNGQDs@AuNPs, and GCE/CoP-BNF/SNGQDs@AuNPs) was immersed in a solution of NHS (0.3 mL, 100 mM) and EDC (0.1 mL, 50 mM) and were stored for 2 h at 4 °C. In the next step the anti-HER2 capture probes i.e. Trasmatuzab/HB5 (10 μL) were immobilized on the activated electrodes and left at 4 °C for 8 h. The six electrodes (GCE/CoP-BNF/HB5, GCE/CoP-BNF/Trasmatuzab, GCE/SNGQDs@AuNPs/HB5, GCE/SNGQDs@AuNPs/Trasmatuzab, GCE/CoP-BNF/SNGQDs@AuNPs/HB5, and GCE/CoP-BNF/SNGQDs@AuNPs/Trasmatuzab) were then rinsed with PBS to remove any unbound aptamer/antibody on the electrode surface. All six electrodes were then treated with 1% BSA (bovine serum albumin) to prevent non-specific binding, and again rinsed with PBS. The electrochemical response of the six electrodes in the presence of varying concentrations of the HER2 antigen was measured using the electrochemical impedance spectroscopy (EIS). GCP used for XPS was modified in the same way.

3. Results and discussion

3.1. Electrode surface characterization

3.1.1. Cyclic voltammetry

Cyclic voltammetry and Impedance spectroscopy were used to characterize the modified electrodes. Fig. 2A and B shows the CVs and EIS, respectively, of different modified electrodes in 1 mM $[Fe(CN)]_6^{3-/4-}$ (in 0.1 M KCl). The bare GCE had an anodic to cathodic peak separation (ΔEp) = 68 mV, Table 1, which is closer to the theoretical Nernst value. Higher ΔEp were obtained upon modification: GCE/SNGQDs@AuNPs (386 mV), GCE/CoP-BNF (555 mV) and GCE/CoP-BNF/SNGQDs@AuNPs (437 mV). This might be due to passivation of the electrode by the highly π-conjugated nanomaterials used which might undergo aggregation on the electrode surface. The CVs shows the ferricyanide peaks near 0.35 V - 0.40 V. The peaks near 0.6 are due CoP based processes and occur only for CoP-BNF containing electrodes [19]. The additional peaks present in the CV of the GCE/SNGQDs@AuNPs surface, might be as a result of the oxidation of gold on the surface of the SNGQDs@AuNPs. There were no peaks due to $[Fe(CN)]_6^{3-/4-}$ in the presence of HB5 or Trasmatuzab. The EIS response for a system is represented using the Nyquist plot. Charge transfer resistance (R_{ct}) is the main parameter that characterizes the electrochemical process at the sensor's surface, and is characterized by the semicircle of the Nyquist plot. The surface-binding of non-conductive molecules blocks the electron transfer, causing an increase in R_{ct}. Conversely, the binding of conductive molecules or molecules able to catalyze redox reactions leads to the decrease in R_{ct}. The R_{ct} data for the modified electrodes are in agreement with the obtained CV data, Table 1. The bare GCE, had the highest conductivity as judged by the lowest R_{ct} value (185 Ω), followed by GCE/SNGQDs@AuNPs (381 Ω), GCE/CoP-BNF/SNGQDs@AuNPs (808 Ω), and GCE/CoP-BNF (838 Ω), Table 1. Upon immobilization of the aptamer (HB5) and antibody (Trasmatuzab) capture probes, an increase in the R_{ct} values was observed for all six electrodes. In addition, in the presence of HER2, the R_{ct} values increased further, Table 1. This might be due to the adsorption of the non-conductive protein layers which hindered electron transfer and diffusion of ferricyanide towards the electrode surface. The aptamer containing electrodes (with or without HER2) had better electron transfer compared to those with the antibody, except for GCE/SNGQDs@AuNPs Table 1, Fig. 3. This is due to the known fact that aptamers are more conductive than the antibodies [14].

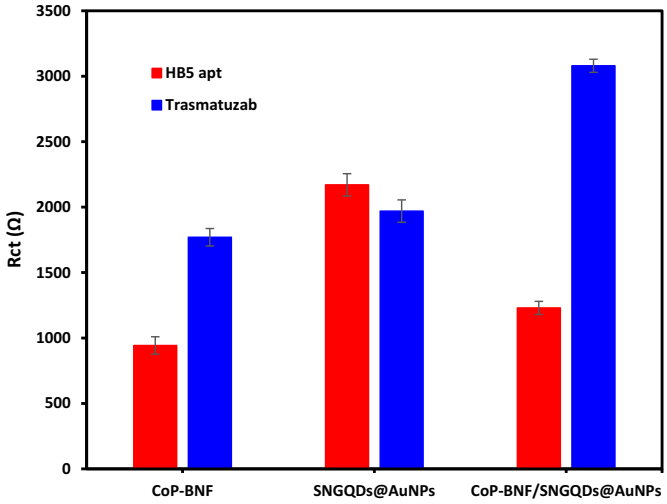

Fig. 3. Bar graphs showing comparative Rct for GCE/CoP-BNF, GCE/SNGQDs@AuNPs, and GCE/CoP-BNF/SNGQDs@AuNPs. All experiments were run in 1 mM $Fe(CN)_6]^{3-/4-}$ in 0.1 mol·L^{-1} KCl in 10 mM PBS (pH 7.4).

3.1.2. X-ray Photoelectron Spectroscopy (XPS)

The structural and chemical evolution of the modified glassy carbon plate (GCP) towards the fabrication of the sensors were assessed using X-ray Photoelectron Spectroscopy (XPS), Fig. S1, Figs. 4 & 5. We focused on the GCP/SNGQDs@AuNPs/HB5 probe and its interaction with the HER2 antigen: Building from the GCP/SNGQDs@AuNPs, following its interaction with HB5 via amide linkage to form GCP/SNGQDs@AuNPs/HB5 and lastly the formation of GCP/SNGQDs@AuNPs/HB5/HER2. The XPS survey spectrum of modified glassy carbon plates was recorded in the range 0–1200 eV, Fig. S1. The GCP/SNGQDs@AuNPs showed four major peaks at 84.64 eV, 163.18 eV, 290.02 eV, 397.14 eV and 535.33 eV, which corresponds to Au_{4f}, S_{2p}, C_{1s}, N_{1s} and O_{1s} respectively. The wide scan spectra (Fig. S1, in Supporting Information) for GCP/SNGQDs@AuNPs/HB5 and GCP/SNGQDs@AuNPs/HB5/HER2 had peaks similar to that of the GCP/SNGQDs@AuNPs surface, accompanied by variations in intensity. The counts/intensities for the GCP/SNGQDs@AuNPs, GCP/SNGQDs@AuNPs/HB5 and GCP/SNGQDs@AuNPs/HB5/HER2 surfaces are listed in Table S1 (Supporting Information). An increase in the intensity of the oxygen, carbon and the sulfur peaks accompanied by a decrease in the nitrogen peak upon attachment of HB5 to GCP/SNGQDs@AuNPs to form GCP/SNGQDs@AuNPs/HB5 was observed, Table. S1 (in supporting information). Attachment of HER2 to GCP/SNGQDs@AuNPs/HB5 resulted in a decrease in intensity of all peaks, Table. S1.

The high resolution C1s spectrum for GCE/SNGQDs@AuNPs showed four peaks at 283.1 eV, 283.6, 284.9 eV and 287.2 eV, which are associated to the functional groups –C-C, C═C, -C-N/C-O and –O-C=O respectively, Table 2. The C1s high resolution XPS spectrum for GCE/SNGQDs@AuNPs/HB5 showed peaks at 283.1 eV (-C=C/-C-C), 284.1 eV (-C-O/-C-N) and 286.9 (O=C-NH), Table 2. The HB5 aptamer is an oligonucleotide and as such might on its own have amide and carboxylic groups. The GCE/SNGQDs@AuNPs/HB5/HER2 surface is due to the interaction between the HB5 aptamer and the HER2 antigen. Biorecognition elements interact with their respective antigens via weak

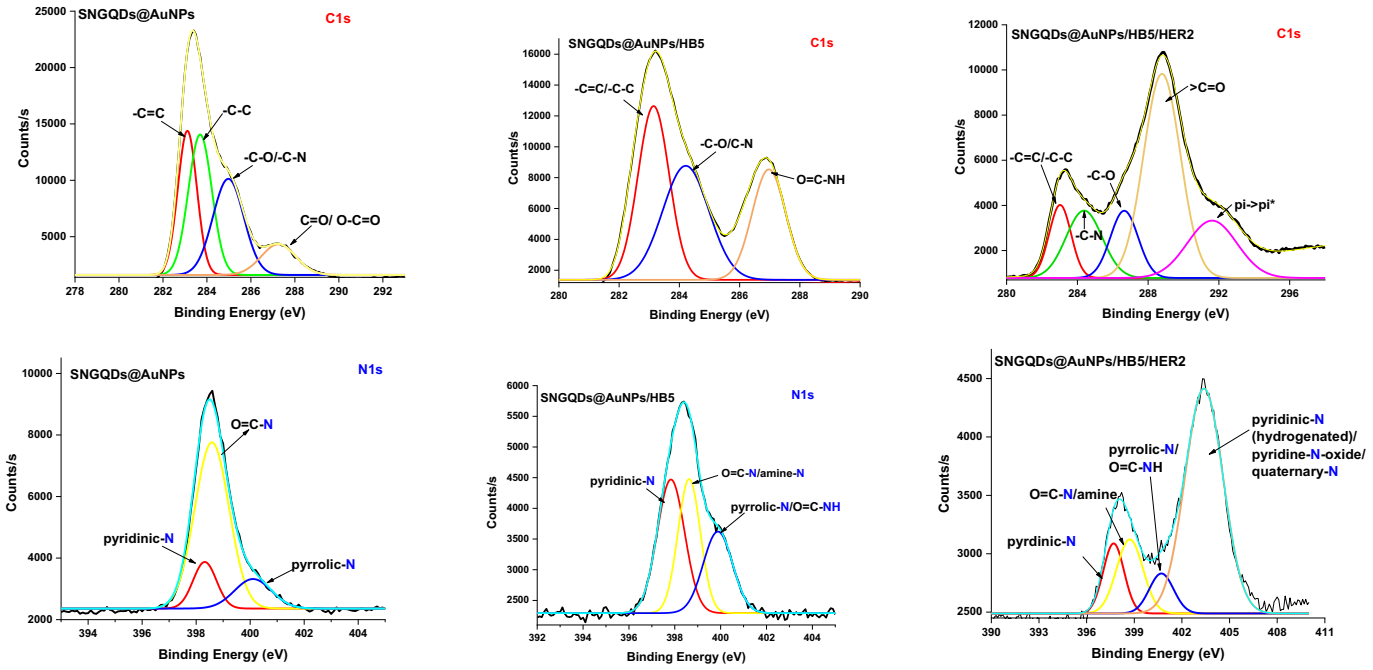

Fig. 4. XPS data showing the high resolution C1s (top) and N1s (bottom) spectra of the modified surfaces GCP/SNGQDs@AuNPs, GCP/SNGQDs@AuNPs/HB5 and GCP/SNGQDs@AuNPs/HB5/HER2 respectively.

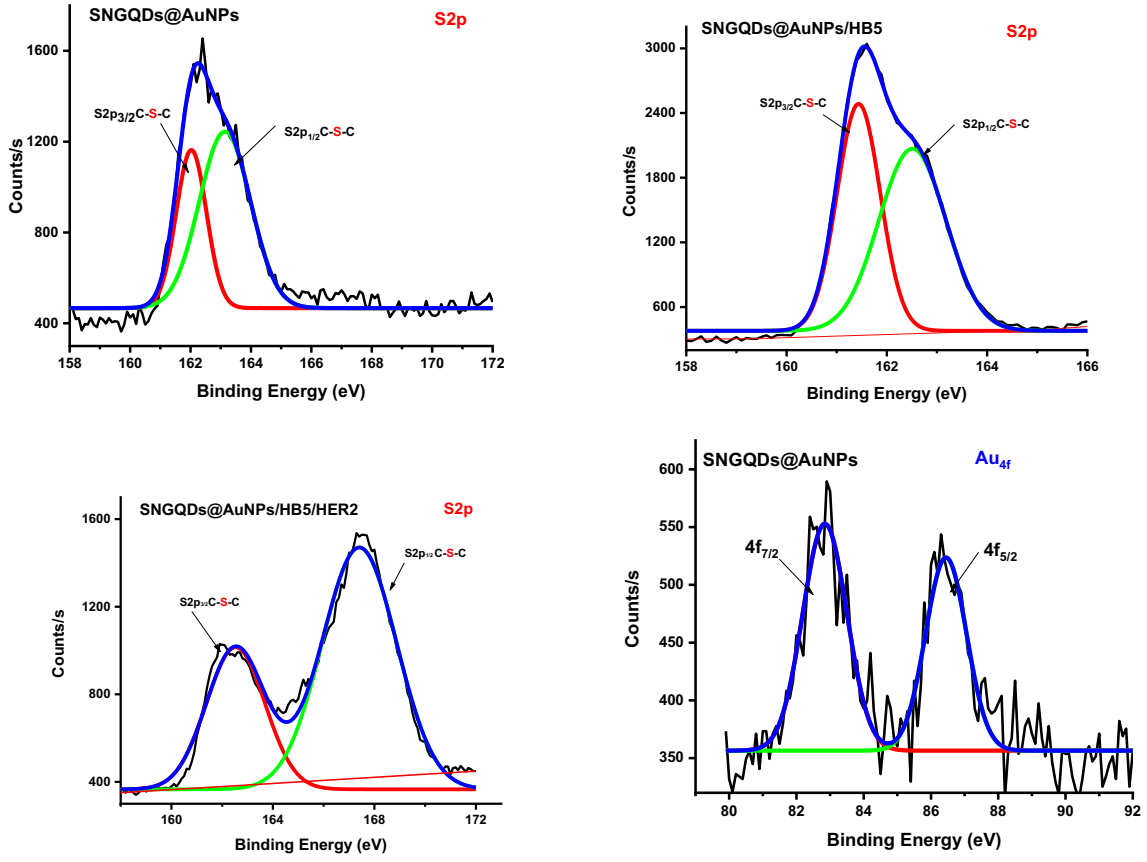

Fig. 5. High resolution S2p spectra for the modified GCP/SNGQDs@AuNPs, GCP/SNGQDs@AuNPs/hb5 and GCP/SNGQDs@AuNPs/HB5/HER2. The figure also shows the high resolution Au_{4f} spectra for SNGQDs@AuNPs.

and non-covalent interactions. An additional peak in the C1s spectra of the GCE/SNGQDs@AuNPs/HB5/HER2 surface at the 292.6 eV was observed, which can be attributed to π-π* peak. The peak might be an indication of the π – π interactions within the SNGQDs@AuNPs framework, and also possibly the π – π interactions relating to the HB5 and HER2 π-electron backbone system, to form a stable hybrid structure on

Table 2
A summary of binding energies (in eV) determined from deconvoluted high resolution XPS spectra.

Electrode[a]	C1s[b]			N1s[b]	S2p (–C-S-C)	
					$S2p_{3/2}$	$S2p_{1/2}$
GCP/SNGQDs@AuNPs	283.1 (-C=C) 283.6 (-C-C)	284.9 (-C-O/-C-N)	287.2 (-O=C-O)	398.3 (Pyridinic-N) 398.5 (O=C-N) 400.1 (Pyrro-N)	162.0	163.8
GCP/SNGQDs@AuNPs/HB5	283.1 (-C=C/-C-C)	284.1 (-C-O/-C-N)	286.9 (O=C-NH)	397.8 (Pyridinic-N) 398.6 (O=C-N) 399.8 (Pyrro-N/ O=C-NH)	161.4	162.5
GCP/SNGQDs@AuNPs/HB5/HER2	283.3 (-C=C/-C-C)	284.4 (-C-N) 286.6 (-C-O)	288.8 (O=C-NH)	397.7 Pyridinic-N) 398.4(O=C-N) 400.7(Pyrro-N/ O=C-NH)	162.5	167.4

[a] GCP = glassy carbon plate.
[b] A single value where more than one functional group is mentioned (e.g. –C=C/-C-C) is associated with peak overlap.

the electrode surface during/upon interaction.

The deconvolution of N 1 s levels for the GCE/SNGQDs@AuNPs sample confirmed the presence of the following nitrogen functional groups: pyridinic-N (398.3 eV), O=C-N (398.5 eV) and pyrrolic-N (400.1 eV). The same peaks were observed for the surface GCE/SNGQDs@AuNPs/HB5. with varied intensities. The three peaks now appeared at the binding energies 397.8 eV, 398.6 eV and 399.8 eV respectively. The peak at 399.9 eV, in the GCE/SNGQDs@AuNPs/HB5 surface is associated with the –O=C-NH (amide nitrogen) functional group, thereby confirming the successful immobilization of the HB5

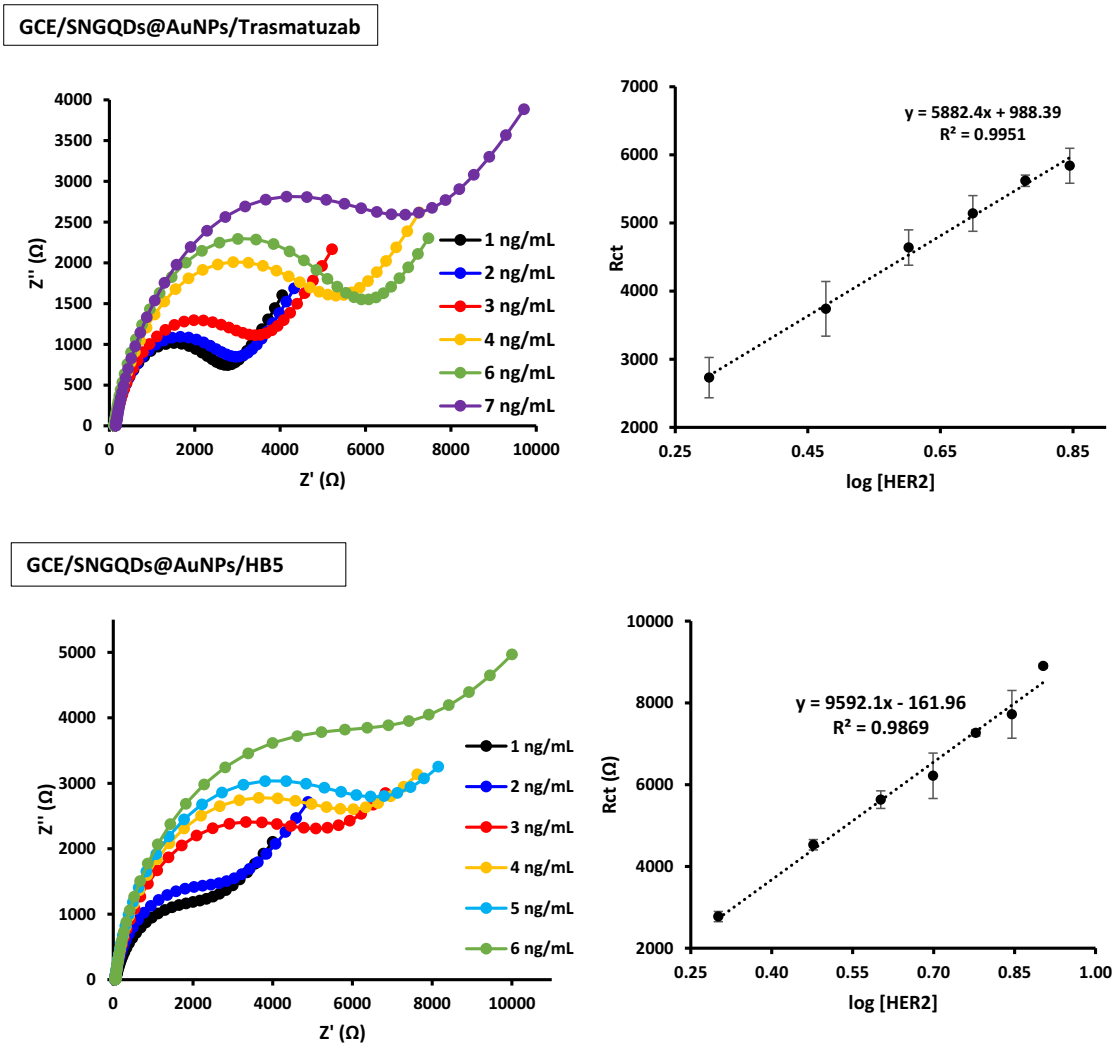

Fig. 6. Nyquist plots and regression plots of log HER2 vs. Rct for all electrodes aptasensor vs. immunosensor. All experiments run in $[Fe(CN)_6]^{3-/4-}$ (1 mM in 0.1 mol·L^{-1} KCl in 10 mM PBS (pH 7.4), showing selected HER2 concentrations.

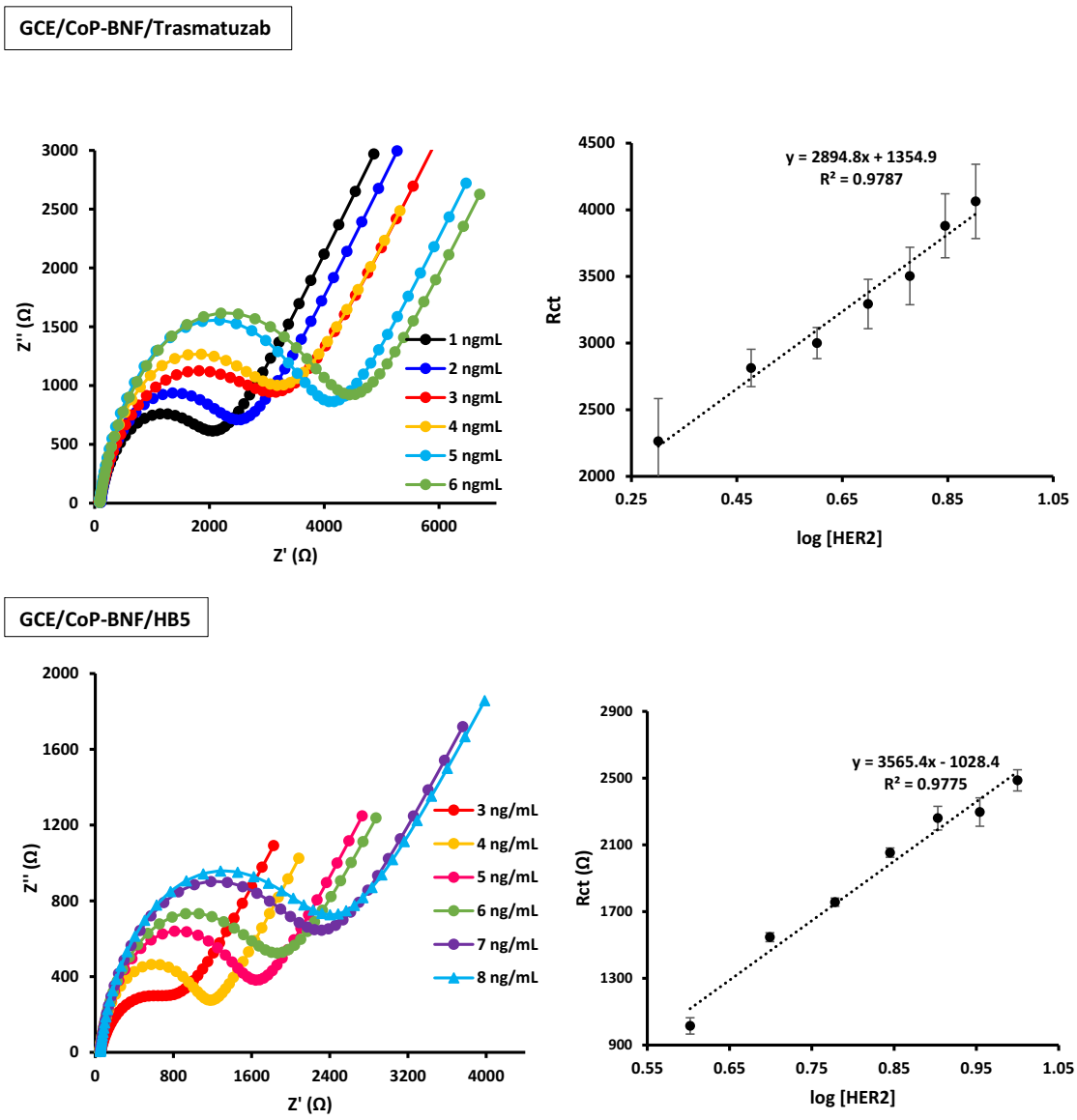

Fig. 6. (*continued*).

aptamer on to the modified electrode surface.

The HB5 aptamer and HER2 antigen interact via non-covalent interactions. As such, the same functional groups were observed for the two GCE/SNGQDs@AuNPs/HB5 and GCE/SNGQDs@AuNPs/HB5/HER2 modified surfaces. The N1s high resolution spectra of the GCE/SNGQDs@AuNPs/HB5/HER2, had the functional group peaks pyridinic-N (397.7 eV), O=C-N (398.4 eV) and pyrrolic-N/O=C-NH (400.7 eV). A new peak was observed at the binding energy 403.3 eV: such energy values can be attributed to oxygenated nitrogen groups, hydrogenation of nitrogen dopants as well as clustered nitrogen substitutions. Hence, the new peak points to the different species and interactions present on the electrode surface, most of which are present in sp^3 coordination, such as hydrogenated and protonated nitrogen from the HER2 protein and the HB5 aptamer, as well as the graphene (including isolated graphitic N defects) [27,28].

The presence of the –C-S-C unit in the SNGQDs structure was confirmed by the high resolution S2p XPS spectra for GCE/SNGQDs@AuNPs, Table 2. The same is observed for the S2p XPS high resolution spectrum for GCE/SNGQDs@AuNPs/HB5, where the two S2p 161.4 eV and 162.5 eV corresponding to the $S2p_{3/2}$ and $S2p_{1/2}$ respectively, were obtained as they were for the GCE/SNGQDs@AuNPs surface, but slightly shifted. The minimal shifts and similar peak integration might imply that the structural integrity of the SNGQDs@AuNPs is maintained during interaction with the HB5 aptamer. The presence of the AuNPs on the surface of the SNGQDs, was further confirmed by the obtained Au 4f core-level spectra, with two peaks at 82.84 eV and 86.44 eV that were assigned as Au $4f_{7/2}$ and Au $4f_{5/2}$, respectively.

3.1.3. *Scanning Electron Microscopy (SEM)*

The SEM analysis of the bare and modified glassy carbon plate (GCP) of the various steps towards immunosensor fabrication has been reported [19] and is shown in Fig. S2. The bare GCP shows a grey surface. The surface for GCP/CoP-BNF show coating of the carbon plate with white crystalline material which might be attributed to the CoP-BNF, Fig. S2b. The GCP/ CoP-BNF/SNGQDs@AuNPs surface shows grey particles on top of the previously formed white CoP-BNF particles, Fig. S2c.

3.2. *Quantitative detection of HER2 in PBS*

The following modified electrodes GCE/CoP-BNF/HB5, GCE/CoP-BNF/Trasmatuzab, GCE/SNGQDs@AuNPs/HB5, GCE/SNGQDs@AuNPs/

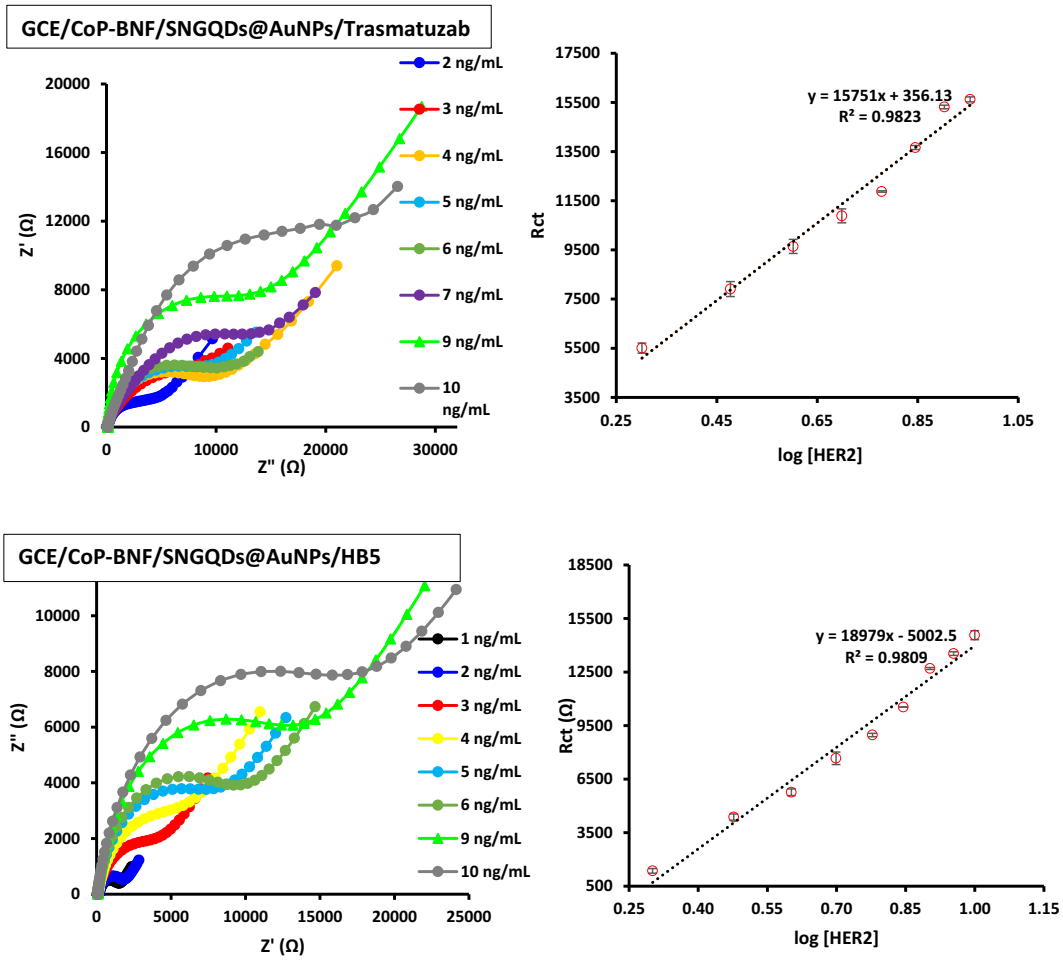

Fig. 6. (*continued*).

Trasmatuzab, GCE/CoP-BNF/ SNGQDs@AuNPs/HB5, GCE/CoP-BNF/ SNGQDs@AuNPs/Trasmatuzab were all tested towards the electrochemical detection of HER2 at varying concentrations of 1 ng to 10 ng in PBS pH 7.4. The stability of HER2 at pH 7.4 has been widely reported in literature, and as such the experiments reported herein were conducted at that pH [29]. Because antibodies are produced using animal models, they are designed to function under physiological conditions, hence pH 7.4 is employed in this work for both aptamers and antibodies. The performance was investigated using the electrochemical impedance spectroscopy (EIS). Thus, the EIS technique was used to study aptamer/antibody-antigen interactions. The Nyquist plots for all six electrodes GCE/CoP-BNF/HB5, GCE/CoP-BNF/Trasmatuzab, GCE/SNGQDs@AuNPs/HB5, GCE/SNGQDs@AuNPs/Trasmatuzab, GCE/CoP-BNF/SNGQDs@AuNPs/HB5, and GCE/CoP-BNF/SNGQDs@AuNPs/Trasmatuzab towards the electrochemical detection of HER2 are shown in Fig. 6. The figures clearly show that there was an increase in R_{ct} with increase in HER2 concentration with all electrodes. This trend held true for both the aptasensors and immunosensors. The increase in R_{ct} signifies a decrease in conductivity. Regression plots were then created using the data of each electrode, the equations of the regression plots were as follows:

(i) GCE/CoP-BNF/HB5: $y = 3565.4x - 1028.4$, $R^2 = 0.9775$
(ii) GCE/CoP-BNF/Trasmatuzab: $y = 2894.8x + 1354.9$, $R^2 = 0.9787$
(iii) GCE/SNGQDs@AuNPs/HB5: $y = 9592.1x - 161.96$, $R^2 = 0.9869$
(iv) GCE/SNGQDs@AuNPs/Trasmatuzab:$y = 5882.4x - 988.93$, $R^2 = 0.9951$

Table 3
Comparative sensitivity and LoD for HER2 detection.

Probe[a]	Sensitivity (kΩ.ng/mL)		LoD (ng/mL		Reference
	Aptasensors (HB5)	Immunosensors (Trasmatuzab)	Aptasensors (HB5)	Immunosensors (Trasmatuzab)	
GCE/SNGQDs@AuNPs	9592.1	5882.4	0.0489	0.1072	This work
GCE/CoP-BNF	3565.4	2894.8	0.0259	0.0454	This work
GCE/ CoP-BNF/ SNGQDs@AuNPs	18,979	15,751	0.0112	0.0327	This work
SPCE/Poly-L-lysine			3		30
GCE/AuNPs			5		31
ITO/SWCNT/Ferrocene/PEI				0.22	32
SPCE/HRP-Enzyme				3	33
ILE/MWCNT-AuNPs				7.4	34

[a] GCE = glassy carbon electrode, SPCE = screen printed carbon electrode, AuNPs = gold nanoparticles, GQDs = graphene quantum dots, ITO = Titanium electrode, PEI = Poly-ethyleneimine, HRP = Horseradish peroxidase enzyme, ILE = ionic liquid electrode, and MWCNT = multiwalled carbon nano tubes.

Table 4
HER2% recovery for the probe GCE/CoP-BNF/SNGQDs@AuNPs.

Aptasensor (HB5)							
[HER2] added	R1	R2	R3	Average	SDEV	% RSD	% [HER2] Recovered
1 ng/mL	1710	1700	1800	1737	45	2.59	142
3 ng/mL	11,630	11,110	11,520	11,420	224	1.96	79
5 ng/mL	19,930	21,920	20,390	20,747	851	4.10	78
7 ng/mL	31,200	31,410	31,080	31,230	136	0.44	96

Immunosensor (Trasmatuzab)							
[HER2] added	Rct 1	Rct 2	Rct 3	Average	Deviation	% RSD	Recovered
1 ng/mL	1888	1970	1840	1899	65.74	3.46	110
3 ng/mL	14,700	14,200	15,000	14,633	404.15	2.76	80
5 ng/mL	21,800	21,700	24,600	22,700	1646.21	7.25	83
7 ng/mL	30,600	28,400	30,200	29,733	1171.89	3.94	91

RSD = % relative standard deviation and SDEV = standard deviation.

(v) GCE/ CoP-BNF/SNGQDs@AuNPs/HB5: $y = 18979x - 5002.5$, $R^2 = 0.9809$
(vi) GCE/ CoP-BNF/ SNGQDs@AuNPs/Trasmatuzab: $y = 15751x + 356.13$, $R^2 = 0.9823$

The slopes (m) of the regression plots give the sensitivity of each sensor/modified electrodes. The aptasensors (HB5 based electrodes) showed better sensitivity compared to the immunosensors (Trasmatuzab based electrodes), Table 3. Limits of detection (LoD) are defined according to the equation $3\sigma_b/m$, where m is the slope of the corresponding calibration curve and σ_b is the standard deviation of the blank. The aptasensors had lower LoD values, compared to its corresponding immunosensor electrodes (Table 3); GCE/CoP-BNF/HB5: Trasmatuzab (0.0489 ng/mL: 0.1072 ng/mL), GCE/SNGQDs@AuNPs/HB5: Trasmatuzab (0.0259 ng/mL: 0.0454 ng/mL) and GCE/CoP-BNF/SNGQDs@AuNPs/HB5: Trasmatuzab (0.0112 ng/mL: 0.0327 ng/mL), Table 3. Aptamers compared to antibodies, are synthetic recognition elements, fine-tuned and designed specifically for the analyte of interest [9]. Their structure is usually optimized to achieve maximum stability, specificity and selectivity. This is further confirmed by the LoD and sensitivity results obtained. The aptasensor/s probes designed in this work had better LoD values, compared to the reported 3 ng/mL and 5 ng/mL values for the RNA aptamer-polylysine [30] and DNA aptamer-gold nanoparticles [31] based aptasensors respectively, for the electrochemical detection of HER2. Similarly, the LoD values for the immunosensors probes in this work showed better LoD values compared to the 0.22 ng/mL, 3 ng/mL, and 7.4 ng/mL obtained for the single walled carbon nanotube and poly-ethyleneimine (SWCNT-PEI)-antibody [32], biotinylated-sandwich-antibody [33] and gold nanoparticle-multiwalled carbon nanotubes (AuNPs-MWCNT)-antibody [34] based immunosensors respectively.

3.3. Detection of HER2 in human serum

The validity and potential applicability of the designed probes in real life was investigated by detection of HER2 in human serum samples. The experiments were done on human (male) blood serum, diluted (1:500 dilution factor) with 10 mM PBS (pH 7.4). Dilution factors as high as 2000 have been reported for the determination of HER2 in human serum [35]. The human serum was spiked with various known concentration of the HER2 antigen (1 ng/mL, 3 ng/mL, 5 ng/mL and 7 ng/mL) respectively.

The different probes were then tested on their ability to detect/recover HER2, in the competitive human serum environment, Table 4 & S2. At the HER2 concentration 1 ng/mL, the HB5 containing surface showed better recoveries at all electrode surfaces, Table S3. At 7 ng/mL, electrodes containing CoP-BNF (GCE/CoP-BNF and GCE/CoP-BNF/SNGQDs@AuNPs) show better recovery for the aptasensor than the immunosensor, Table S3. The results obtained demonstrate the competitiveness of both the antibody and aptamer as capture probes in the design of sensitive biosensors. The smaller size of the aptamer and its ability to fold, poses an advantage for sensing at higher concentrations as seen for the probes GCE/CoP-BNF and GCE/CoP-BNF/SNGQDs@AuNPs. Antibodies are susceptible to pH changes and

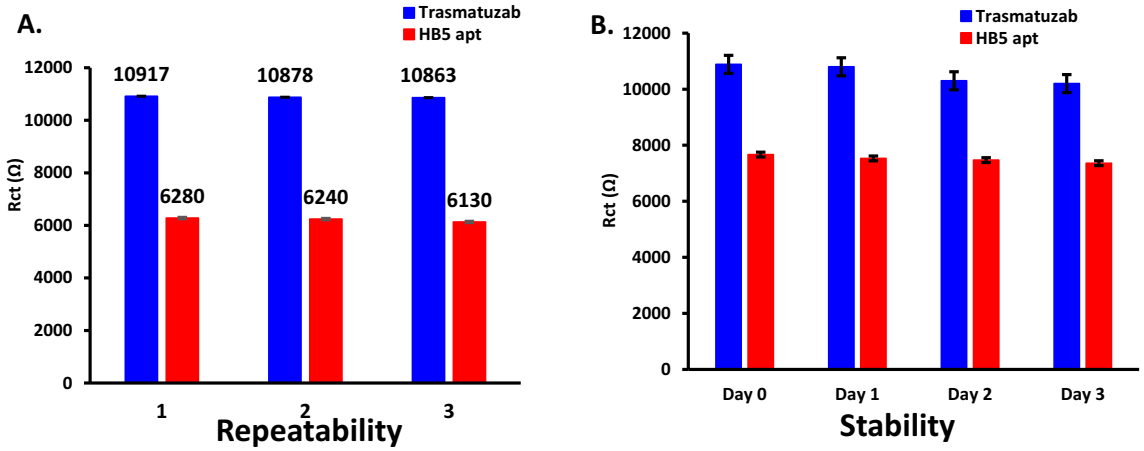

Fig. 7. (A) Repeatability of the GCE/SNGQDs@AuNPs/Trasmatuzab/HER2 and GCE/SNGQDs@AuNPs/HB5/HER for (n = 3 cycles), and (B) Stability of the best performing aptasensor and immunosensor probes: GCE/CoP-BNF/SNGQDs@AuNPs/Trasmatuzab and GCE/CoP-BNF/SNGQDs@AuNPs/HB5 over 3 days, all at HER2 concentration 5 ng/mL. All experiments were run in 1 mM $Fe(CN)_6]^{3-/4-}$ in 0.1 mol·L^{-1} KCl in 10 mM PBS (pH 7.4).

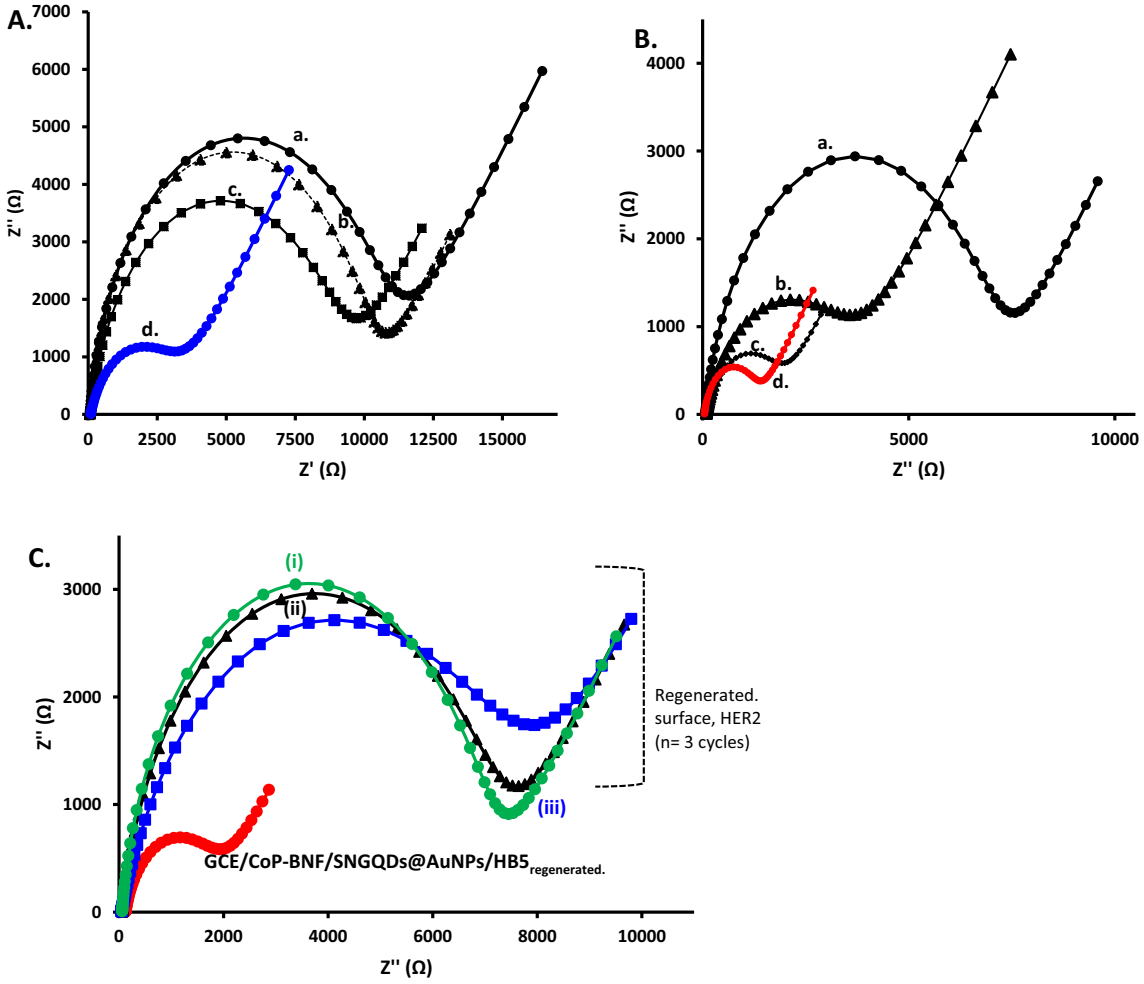

Fig. 8. Nyquist plots obtained from surface regeneration of the probes: (A) GCE/CoP-BNF/SNGQDs@AuNPs/Trasmatuzab and (B) GCE/CoP-BNF/SNGQDs@AuNPs/HB5 respectively. Where in both plots (a) represents the electrodes coupled with HER2 (5 ng/mL) prior acid treatment, (b) and (c) electrode surfaces after acid (pH 2) treatment for 5 min and 15 min respectively and (d) the respective probes without HER2. Fig. 8C shows the successfully regenerated (using pH 7.4 buffer) GCE/CoP-BNF/SNGQDs@AuNPs/HB5 surface towards HER2 (5 ng/mL) detection, (n = 3 cycles, i ii, and iii).

denatured antibodies cannot be repaired, while aptamers are fairly stable and are easily refolded if denatured, hence better recoveries for the latter.

3.4. Stability and repeatability

The stabilities of the designed immunosensor and aptasensor were tested and compared using the best electrodes of each (in terms of LoD): GCE/CoP-BNF/SNGQDs@AuNPs/HB5 and GCE/CoP-BNF/SNGQDs@AuNPs/Trasmatuzab, when comparing the respective HB5 and Trasmatuzab containing electrodes. The electrodes were prepared and stored for 3 days at 4 °C, and monitored daily, Fig. 7B. There R_{ct} values were retained as the first day up to 96% for the aptasensor, and 97% for the immunosensor. The repeatability of the designed immunosensors and aptasensors is demonstrated throughout, the experiments were run ($n = 3$) at all concentrations for all six electrodes, Table S4. Fig. 7A, shows the repeatability of the electrodes GCE/CoP-BNF/SNGQDs@AuNPs/HB5 and GCE/CoP-BNF/SNGQDs@AuNPs/Trasmatuzab at HER2 concentration of 5 ng/mL, with the relative standard deviation less than 2% for both probes, Fig. 7A. All electrodes showed similar electrochemical response with acceptable relative standard deviations for biosensors.

3.5. Surface regeneration

Surface regeneration in biosensors can be defined as the ability to regenerate a sensing surface to allow for reusability. The reusability of any sensor is a promise to an inexpensive sensor design and development. Efficient regeneration involves the removal of a bound analyte while preserving the integrity of the ligand/capture probe [36,37]. This quality of biosensors is highly dependent on the structural qualities of the capture probe, which then influences the surface of the sensor. Aptamers compared to antibodies are structurally malleable and can exist in distinct conformations under various conditions [38]. To investigate this advantage of aptamers in biosensor design and efficiency, the surface regeneration of the biosensor was studied. We explored and compared the regeneration efficiency of the antibody-HER2 antigen and aptamer-HER2 antigen surfaces, Fig. 8. The successful regeneration of the electrode surfaces was investigated based on three conditions: (i) the stability of the surface chemistry of the biosensor before and after dissociation, (ii) the ability of the antibody-HER2 or aptamer-HER2 interaction to dissociate fully under the set conditions, and (iii) the stability of the capture probes (aptamer/antibody) and their ability to retain activity and detect the analyte after regeneration. The electrodes GCE/CoP-BNF/ SNGQDs@AuNPs/HB5/HER2 and GCE/CoP-BNF/SNGQDs@AuNPs/Trasmatuzab/HER2 ([HER2] =5 ng/mL) as the best performing probes were investigated. The capture probes (aptamer/antibody)-HER2 antigen were disrupted

using the chemical method. pH = 2.0 and 7.4 PBS buffers were employed for dissociation and regeneration, respectively. The probes were subjected to a pH 2 PBS buffer to render the desorption of the HER2 antigen off of the surfaces. The electrodes were then rinsed with pH 7.4 PBS buffer to restore the conformation and integrity of the capture probes where possible, prior to proceeding to the next cycle of measurement. The two sensor probes GCE/CoP-BNF/SNGQDs@AuNPs/HB5 $_{original}$/HER2 (R_{ct} = 7040 Ω) and GCE/CoP-BNF/SNGQDs@AuNPs/Trasmatuzab $_{original}$/HER2 (R_{ct} = 10,570 Ω) were incubated with pH 2 PBS buffer for 15 min. The % dissociation were calculated as follows:

$$\%dissociation = \frac{R_{ct\ (before\ treatment)} - R_{ct\ (after\ treatment)}}{R_{ct\ (before\ treatment)}} \times 100$$

where treatment means incubation with pH 2 PBS buffer.

The progress of the capture probe-antigen dissociation was checked first at 5 min, to which the GCE/CoP-BNF/SNGQDs@AuNPs/Trasmatuzab/HER2$_{t=5min}$ (R_{ct} = 10,193 Ω) probe had % dissociation of 4%, while the GCE/CoP-BNF/SNGQDs@AuNPs/HB5/HER2$_{t=5min}$ (R_{ct} = 3213 Ω) probe had % dissociation of 54%. After 15 min had elapsed, the GCE/CoP-BNF/ SNGQDs@AuNPs/Trasmatuzab/HER2$_{t=15min}$ (R_{ct} = 9106 Ω) had a % dissociation of 14%, and the GCE/CoP-BNF/SNGQDs@AuNPs/HB5/HER2$_{t=15min}$ (R_{ct} = 1227 Ω) with a % dissociation of 83%. To determine how much of the surface was regenerated, we looked at the probes before coupling with HER2 i.e. GCE/CoP-BNF/SNGQDs@AuNPs/HB5 (R_{ct} = 1147 Ω) and GCE/CoP-BNF/SNGQDs@AuNPs/Trasmatuzab (R_{ct} = 3250 Ω) and compared them to the R_{ct} values obtained after the 15 min of acid treatment had elapsed. Based on the R_{ct} values, it is obvious that the HB5 aptamer containing surface probe was regenerated, compared to that of the Trasmatuzab. The regenerated surface GCE/CoP-BNF/SNGQDs@AuNPs/HB5$_{regenerated}$ (R_{ct} = 1227 Ω), was tested for its reusability by detection of HER2 at 5 ng/mL: GCE/CoP-BNF/ SNGQDs@AuNPs/HB5$_{regenerated}$/HER2, Fig. 8C. The R_{ct} value obtained for the new surface (7313 Ω) was similar to that of the GCE/CoP-BNF/SNGQDs@AuNPs/HB5 $_{original}$/HER2 (R_{ct} = 7040 Ω) probe, Fig. 8B. The results obtained showed the superiority of aptamers compared to antibodies as a capture probe, where surface regeneration, reusability and cost effectiveness are concerned.

4. Conclusions

In this work we report on a comparative study for label-free GCE based impedimetric biosensing platforms prepared using both an antibody and aptamer as bioreceptors. The platforms showed sensitivity and reproducibility towards the HER2 antigen as the analyte. The superiority of the aptamer as a bioreceptor compared to the antibody was shown in sensitivity, LoD values and surface regeneration. We were able to show the surface regeneration on the aptamer based probe, GCE/CoP-BNF/SNGQDs@AuNPs/HB5 compared to its counter antibody based GCE/CoP-BNF/SNGQDs@AuNPs/Trasmatuzab probe. This further elevated the aptamer as an alternative bioreceptor in electrochemical based HER2 detection concerning reusability and cost effectiveness. The characterization and comparison of the dynamic biosensor attributes (stability, repeatability, linearity, and sensitivity) of the aptasensor and immunosensor probes were successfully performed. As such, the results obtained prove the respective competitiveness of the aptamer and antibody as capture probes in biosensing design. Our study suggests some advantages of aptasensor in terms of better stability, simplicity and cost effectiveness. In addition, the obtained LOD values were lower than 15 ng/mL which is the cut off concentration of the HER2 protein in normal cells, rendering the sensors herein as prospects in the application of early stage breast cancer diagnosis.

Credit authorship contribution statement

Sixolile Centane: Conceptualization, Investigation, Writing of original draft, Methodology, Data curation. Tebello Nyokong: Supervision, Resources, reviewing, editing, funding acquisition.

Declaration of Competing Interest

The authors declare that they have no known competing financial interests or personal relationships that could have appeared to influence the work reported in this paper.

The authors declare the following financial interests/personal relationships which may be considered as potential competing interests:

Acknowledgements

This work was supported by the National Research Foundation (NRF) of South Africa through DSI/NRF South African Research Chairs Initiative for Professor of Medicinal Chemistry and Nanotechnology (UID 62620), and Rhodes University.

Appendix A. Supplementary data

Supplementary data to this article can be found online at https://doi.org/10.1016/j.jinorgbio.2022.111764.

References

[1] D.C. Kim, D.J. Kang, Molecular recognition and specific interactions for biosensing applications, Sensors (Basel.) 8 (2008) 6605–6641.
[2] Q. Gu, W. Nanney, H.H. Cao, H. Wang, T. Ye, Single molecule profiling of molecular recognition at a model electrochemical biosensor, J. Am. Chem. Soc. 140 (2018) 14134–14143.
[3] H.L.L. Yu, A. Maslova, I.-M. Hsing, Rational design of electrochemical DNA biosensors for point-of-care applications, Chem.ElectroChem 4 (2017) 795–805.
[4] V. Crivianu-Gaita, M. Thompson, Aptamers, antibody scFv, and antibody fab' fragments: an overview and comparison of three of the most versatile biosensor biorecognition elements, Biosens. Bioelectron. 85 (2016) 32–45.
[5] P.J. Conroy, S. Hearty, P. Leonard, R.J. O'Kennedy, Antibody production, design and use for biosensor-based applications, Semin. Cell Dev. Biol. 20 (2009) 10–26.
[6] M. Labib, E.H. Sargent, S.O. Kelley, Electrochemical methods for the analysis of clinically relevant biomolecules, Chem. Rev. 116 (2016) 9001–9090.
[7] K. Hanack, K. Messerschmidt, M. Listek, in: T. Böl-Dicke (Ed.), Protein Targeting Compounds: Prediction, Selection and Activity of Specific Inhibitors, Springer International Publishing, Cham, 2016, pp. 11–22.
[8] B. Byrne, E. Stack, N. Gilmartin, R. O'Kennedy, Antibody-based sensors: principles, problems and potential for detection of pathogens and associated toxins, Sensors 9 (2009) 4407–4445.
[9] S. Song, L. Wang, J. Lia, C. Fan, J. Zhao, Aptamer-based biosensors, trends, Anal. Chem. 27 (2008) 108–117.
[10] W. Zhou, P.J. Huang, J. Ding, J. Liu, Aptamer-based biosensors for biomedical diagnostics, Analyst 193 (2014) 2627–2640.
[11] M. Citartan, T.-H. Tang, Recent developments of aptasensors expedient for point-of-care (POC) diagnostics, Talanta 199 (2019) 556–566.
[12] Y. Ning, J. Hu, F. Lu, Aptamers used for biosensors and targeted therapy, Biomed. Pharmacother. 132 (2020), https://doi.org/10.1016/j.biopha.2020.110902.
[13] A. Dhiman, P. Kalra, V. Bansal, J.G. Bruno, T.K. Sharma, Aptamer-based point-of-care diagnostic platforms, Sens. Actuators B Chem. 246 (2017) 535–553.
[14] P. Dhar, R.M. Samarasinghe, S. Shigdar, Antibodies, Nanobodies, or Aptamers—which is best for deciphering the proteomes of non-model species? Int. J. Mol. Sci. 21 (2021) https://doi.org/10.3390/ijms21072485.
[15] M. Srivastava, N.R. Nirala, S.K. Srivastava, R. Prakash, A comparative study of Aptasensor Vs Immunosensor for label-free PSA Cancer detection on GQDs-AuNRs modified screen-printed electrodes, Sci. Rep. 8 (2018), https://doi.org/10.1038/s41598-018-19733-z.
[16] C. Yao, T. Zhu, Y. Qi, Y. Zhao, H. Xia, W. Fu, Development of a quartz crystal microbalance biosensor with Aptamers as bio-recognition element, Sensors 10 (2010) 5859–5871.
[17] U. Schlecht, A. Malavé, T. Gronewold, M. Tewes, M. Löhndorf, Comparison of antibody and aptamer receptors for the specific detection of thrombin with a nanometer gap-sized impedance biosensor, Anal. Chim. Acta 573–574 (2006) 65–68.
[18] B.I. Escudero-Abarca, S.H. Suh, M.D. Moore, H.P. Dwivedi, L.-A. Jaykus, Selection, characterization and application of nucleic acid Aptamers for the capture and detection of human Norovirus strains, PLoS One 9 (2014) 1–11.
[19] S. Centane, T. Nyokong, The antibody assisted detection of HER2 on a cobalt porphyrin binuclear framework and gold functionalized graphene quantum dots modified electrode, J. Electroanal. Chem. 880 (2020), https://doi.org/10.1016/j.jelechem.2020.114908.
[20] N.T.N. Anh, R. Doong, One-step synthesis of size-tunable gold@sulfur-doped Graphene quantum dot Nanocomposites for highly selective and sensitive detection

of Nanomolar 4-Nitrophenol in aqueous solutions with complex matrix, ACS Appl. Nano Mater. 1 (2018) 2153–2163.
[21] T. Fan, G. Zhang, L. Jian, I. Murtaza, H. Meng, Y. Liu, Y. Min, Facile synthesis of defect-rich nitrogen and sulfur co-doped graphene quantum dots as metal-free electrocatalyst for the oxygen reduction reaction, J. Alloys. Compounds 792 (2019) 844–850.
[22] K.M. Kadish, E. Van Caemelbecke, Electrochemistry of porphyrins and related macrocycles, J. Solid State Electrochem. 7 (2003) 254–258.
[23] T. Tanaka, A. Osuka, Conjugated porphyrin arrays: synthesis, properties and applications for functional materials Chem, Soc. Rev 44 (2015) 943–969.
[24] S. Brüller, H.-W. Liang, U.I. Kramm, J.W. Krumpfer, X. Feng, K. Müllen, Bimetallic porous porphyrin polymer-derived non-precious metal electrocatalysts for oxygen reduction reactions, J. Mater. Chem. A 3 (2015) 23799–23808.
[25] X. Yan, Y. Song, J. Liu, N. Zhou, C. Zhang, L. Heb, Z. Zhang, Z. Liuc, Two-dimensional porphyrin-based covalent organic framework: a novel platform for sensitive epidermal growth factor receptor and living cancer cell detection, Biosens. Bioelectron. 126 (2019) 734–742.
[26] S. Muniappan, S. Lipstman, S. George, I. Goldberg, Porphyrin framework solids. Synthesis and structure of hybrid coordination polymers of Tetracarboxyphenyl porphyrins and lanthanide-bridging ions, Inorg. Chem. 46 (2007) 5544–5554.
[27] K. Artyushkova, Misconceptions in interpretation of nitrogen chemistry from x-ray photoelectron spectra, J. Vac. Sci. Technol. A 38 (2020), 031002, https://doi.org/10.1116/1.5135923.
[28] T. Susi, T. Pichler, P. Ayala, X-ray photoelectron spectroscopy of graphitic carbon Nanomaterials doped with heteroatoms, Beilstein J. Nanotechnol. 6 (2015) 177–192.
[29] M.W. Traxlmayr, E. Lobner, C. Hasenhindl, G. Stadlmayr, C. Oostenbrink, F. Rüker, C. Obinger, Construction of pH-sensitive Her2-binding IgG1-fc by directed evolution, Biotechnol. J. 9 (2014) 1013–1022.
[30] G. Bezerra, C. Córdula, D. Campos, G. Nascimento, N. Oliveira, M.A. Seabra, V. Visani, S. Lucas, I. Lopes, J. Santos, F. Xavier Jr., M.A. Borba, D. Martins, J. Lima-Filho, Electrochemical aptasensor for the detection of HER2 in human serum to assist in the diagnosis of early stage breast cancer, J. Anal. Bioanal. Chem. 411 (2019) 6667–6676.
[31] L. Chun, S.-E. Kim, M. Choa, W. Choe, J. Nam, D.W. Lee, Y. Lee, Electrochemical detection of HER2 using single stranded DNA aptamer modified gold nanoparticles electrode, Sens. Actuators B Chem. 186 (2013) 446–450.
[32] H. Zhong, C. Zhao, J. Chen, M. Chen, T. Luo, R.W. Tang, J. Liu, Electrochemical immunosensor with surface-confined probe for sensitive and reagentless detection of breast cancer biomarker, RSC Adv. 10 (2020) 22291–22296.
[33] S.D. Tallapragada, K. Layek, R. Mukherjee, K.K. Mistry, M. Ghosh, Development of screen-printed electrode based immunosensor for the detection of HER2 antigen in human serum samples, Bioelectrochemistry 118 (2017) 25–30.
[34] E. Arkan, R. Saber, Z. Karimi, M. Shamsipur, A novel antibody-antigen based impedimetric immunosensor for low level detection of HER2 in serum samples of breast cancer patients via modification of a gold nanoparticles decorated multiwall carbon nanotube-ionic liquid electrode, Anal. Chim. Acta 874 (2015) (2015) 66–74.
[35] L. Maple, R. Lathrop, S. Bozich, W. Harman, R. Tacey, M. Kelley, A. Danilkovitch-Miagkova, Development and validation of ELISA for Herceptin detection in human serum, J. Immunol. Methods 295 (2004) 169–182.
[36] J.A. Goode, J.V.H. Rushworth, P.A. Millner, Biosensor regeneration: a review of common techniques and outcomes, Langmuir 31 (2015) 6267–6276.
[37] S. Arshavsky-Graham, K. Urmann, R. Salama, N. Massad-Ivanir, J.-G. Walter, T. Scheper, E. Segal, Aptamers vs. antibodies as capture probes in optical porous silicon biosensors, Analyst 145 (2020) 4991–5003.
[38] H. Zhao, L.F. Boyd, P. Schuck, Measuring protein interactions by optical biosensors, Curr. Protoc. Protein Sci. 88 (2017) 20.2.1–20.2.25, https://doi.org/10.1002/cpps.31.